

A Model for the Evolution of the Elemental Abundances of Solar Energetic Particles

Chee K. Ng^{1,2}, Donald V. Reames¹, and Allan J. Tylka³

¹Laboratory for High Energy Astrophysics, NASA/GSFC, Greenbelt, MD 20771, USA

²Department of Astronomy, University of Maryland, College Park, MD 20742, USA

³E. O. Hulburt Center for Space Science, Naval Research Laboratory, Washington, DC 20375, USA

Abstract

We present a theoretical model of the coupled evolution of the phase space densities of solar energetic particles (SEP) and interplanetary Alfvén wave distribution for interpreting the evolution of elemental abundances in SEP accelerated by a traveling interplanetary shock. The model is formulated in “mixed” coordinates and includes the effects of magnetic focusing, pitch-angle scattering, solar-wind convection, and adiabatic deceleration, as well as wave transport and amplification by streaming protons. The results suggest that a key ingredient for understanding SEP abundance variation is the transport of shock accelerated ions through proton excited non-Kolmogorov wave spectra.

1 Introduction

The acceleration and transport of SEP has long been a challenge for theoretical modeling because of the variety and complexity of the physical processes involved (Lee, 1997; Reames, 1999). Despite the difficulties, the challenge must be met not only for theoretical interest but also for interpreting SEP observations. The pressing need for a realistic model is manifest when we attempt to understand the systematic variations of SEP abundances observed by the sensitive Wind/EPACT instrument (Tylka, Reames & Ng, 1999a,b). The temporal variations of SEP abundances explore the *differences* in the acceleration and transport experienced by SEP ions of different A/Q ratios (A = atomic mass, Q = charge state), and challenge our ingenuity in separating the roles played by source abundances, charge states, acceleration and interplanetary transport. We have taken two important steps in modeling the evolution of ion phase space densities by including (i) the effect of self excited waves on SEP transport (Ng & Reames, 1994), and (ii) a moving source of energetic ions associated with a traveling shock (Ng, Reames & Tylka, 1999). In this paper, we present preliminary results from our newest model which now includes the effects of solar-wind convection on ions and waves, and adiabatic deceleration. The new results support our earlier suggestion that ion transport through proton amplified waves is key to understanding the temporal evolution of SEP abundances.

2 Model and Equations

The model includes magnetic focusing, pitch-angle scattering, wave amplification, energetic ion source at a traveling “shock”, solar-wind convection of waves and ions, and adiabatic deceleration. We make several simplifications to render the model tractable. Acceleration is decoupled from transport by injecting time varying power-law energetic ion spectra at a “shock” that travels with constant velocity V_{sh} on a radial magnetic field. The phase-space densities $f_s(\mu, P, r, t)$ of ion species s and the differential magnetic energy density $I_\sigma(k, r, t)$ of σ -mode Alfvén wave satisfy the following differential equations in “mixed coordinates”: (r, t) in fixed inertial frame and (μ, P) in the solar-wind frame.

$$\frac{\partial F_s}{\partial t} + \frac{\partial}{\partial r}[(\mu v + W)F_s] + \frac{\partial}{\partial \mu} \left[\frac{1 - \mu^2}{r} (v + \mu W) F_s \right] - P \frac{\partial}{\partial P} \left[\frac{1 - \mu^2}{r} W F_s \right] - \frac{\partial}{\partial \mu} \left[D_{\mu\mu}^s \frac{\partial F_s}{\partial \mu} \right] = G_s \quad (1)$$

$$\frac{\partial \Psi_\sigma}{\partial t} + \frac{\partial}{\partial r} (V_\sigma \Psi_\sigma) + \frac{\partial}{\partial \eta} \left[\left(2 \frac{V_\sigma}{r} - \frac{dV_\sigma}{dr} \right) \Psi_\sigma \right] = \gamma_\sigma \Psi_\sigma \quad (2)$$

$$D_{\mu\mu}^s = \frac{v^2}{4P^2} \sum_{\sigma} \int dk I_{\sigma}(k, r, t) R_{\mu\mu}^{\sigma}(\mu, v, P, k, V_{\sigma}) \quad (3)$$

$$\gamma_{\sigma} = 2\pi^2 g_{\sigma} e^3 c V_A \iint d\mu dP \frac{P^3}{E^2} \frac{R_{\mu\mu}^{\sigma}}{(1 - \mu V_{\sigma}/v)^2} \frac{\partial f_H}{\partial \mu} \quad (4)$$

$$F_s(\mu, P, r, t) = \frac{B_0}{B} \left(\frac{P}{P_{0,s}} \right)^3 f_s(\mu, P, r, t) \quad \text{and} \quad \Psi_{\sigma}(k, r, t) = \frac{k}{k_0} \frac{B_0}{B} \frac{V_{\sigma}}{V_A} 2I_{\sigma}(k, r, t).$$

In the above, t is time, r heliocentric distance, v ion velocity, P rigidity, μ pitch-angle cosine, $D_{\mu\mu}^s(P, \mu, r, t)$ species- s diffusion coefficient in μ -space, $B = B_0(r_0/r)^2$ magnetic field, k wavenumber, $\eta = \ln(k/B)$, G_s ion source term, γ_{σ} growth rate of I_{σ} , c light speed, e elementary charge, E proton total energy, $V_A \propto r^{-1}$ Alfvén speed, W solar-wind speed, V_{sh} shock speed, $r_{sh} = r_{0,sh} + tV_{sh}$ shock distance from Sun, $V_{\sigma} = W + g_{\sigma}V_A$, $g_{\sigma} = \pm 1$ for outward (inward) waves, B_0 , k_0 , r_0 and $r_{0,sh}$ are constants, and $R_{\mu\mu}^{\sigma}(\mu, v, P, k, V_{\sigma})$ is the wave-particle resonance function (Ng & Reames, 1995). In eq. (1), the third, fourth and fifth terms represent the effects of focusing, adiabatic deceleration, and pitch-angle diffusion respectively. See Ruffolo(1995), Barnes (1979) for further discussion on eqs. (1) and (2), respectively. Only f_H appears in eq. (4) since the minor ions contribute negligibly to wave evolution (Lee, 1983). Eq. (1) for f_H and eq. (2) for I_{σ} are coupled via eqs. (3) and (4). The ion source G_s per ($\text{cm}^2 \text{MV}^3 \text{h}$) is assumed isotropic and sharply peaked at $r = r_{sh}$, such that

$$\frac{1}{\Delta r} \int_{r_{sh}-\Delta r/2}^{r_{sh}+\Delta r/2} G_s dr = a |\alpha| \frac{n_s(r_0) r_0^2}{P_{0,s}^3 r_{sh}^2} \left(\frac{P}{P_{0,s}} \right)^{\alpha} \quad (5)$$

and G_s is negligible outside $(r_{sh} - \Delta r/2, r_{sh} + \Delta r/2)$, with Δr the finite-difference grid size. In eq. (5), $n_s(r_0)r_0^2/r^2$ is the solar-wind s -ion density at r , $r_0 \equiv 1 \text{ AU}$, $P_{0,s}$ is the “seed” ion rigidity, and we set $a = 8 \times 10^{-5} \text{ h}^{-1}$ for all ion species. We take $n_H(r_0)$, $n_O(r_0)$ and $n_{Fe}(r_0)$ in proportion to the observed coronal abundances (Reames, 1995), e.g. 6.4 cm^{-3} , $4.1 \times 10^{-3} \text{ cm}^{-3}$ and $5.5 \times 10^{-4} \text{ cm}^{-3}$, respectively. All ions are seeded at the same 5 keV/amu (Lee, 1983).

For the results in Section 3, we start with empty ion distributions and forward propagating right and left-hand polarized Alfvén wave intensities which are steady-state solutions of eq.(2) with Kolmogorov spectra, such that the ion mean free paths $\lambda = 3/8 \int_{-1}^1 d\mu (1 - \mu^2)^2 v / D_{\mu\mu} > 1 \text{ AU}$ in the inner heliosphere. At $t = 0$, a “shock” travels out at specified velocity V_{sh} , releasing energetic ions with spectral index $\alpha = \delta + \beta V_{sh} t$ (eq.[5]). Classical shock acceleration theory gives $\alpha = -3c_r/(c_r - 1)$, with c_r the compression ratio, and $\alpha = -4$ for the maximum $c_r = 4$. The coupled eqs. (1) and (2) are solved using a refinement of the finite-difference techniques described in Ng & Reames (1994). In Section 3 we study how the Fe/O and He/H ratios depend on the shock-related source strength.

3 Results

We study the evolution of Fe/O at 2.6, 3.7, and 5.2 MeV/amu, and He/H at 2.2 MeV/amu, in the energy range reported by Tylka et al. (1999a,b). We take $A_{Fe}/Q_{Fe} = 4$, $A_O/Q_O = A_{He}/Q_{He} = 2$. The calculated abundance ratios are displayed versus time in Fig. 1(a)-(d). In all cases, all Fe/O ratios decrease precipitously after event onset. For moderately strong but fast weakening shock (a), they continue to decrease at slower rates, punctuated by a brief small “shock spike”. For maximum compression shock that weakens rapidly (b), all Fe/O ratios rebound to energy-dependent values > 2 , then decrease to < 1 , faster at higher energy. For the persistent maximum compression shock (c), all Fe/O ratios rebound to ≈ 2 , decaying very slowly past unity at shock passage. The energy dependence of Fe/O is different in case (c) than cases (a) and (b).

At onset, He/H decreases rapidly like Fe/O for the weak shock in Fig. 1(a), but *rises* sharply for the stronger shocks in (b) and (c). Since at the same MeV/amu, He^{2+} (Fe^{14+}) has higher rigidity

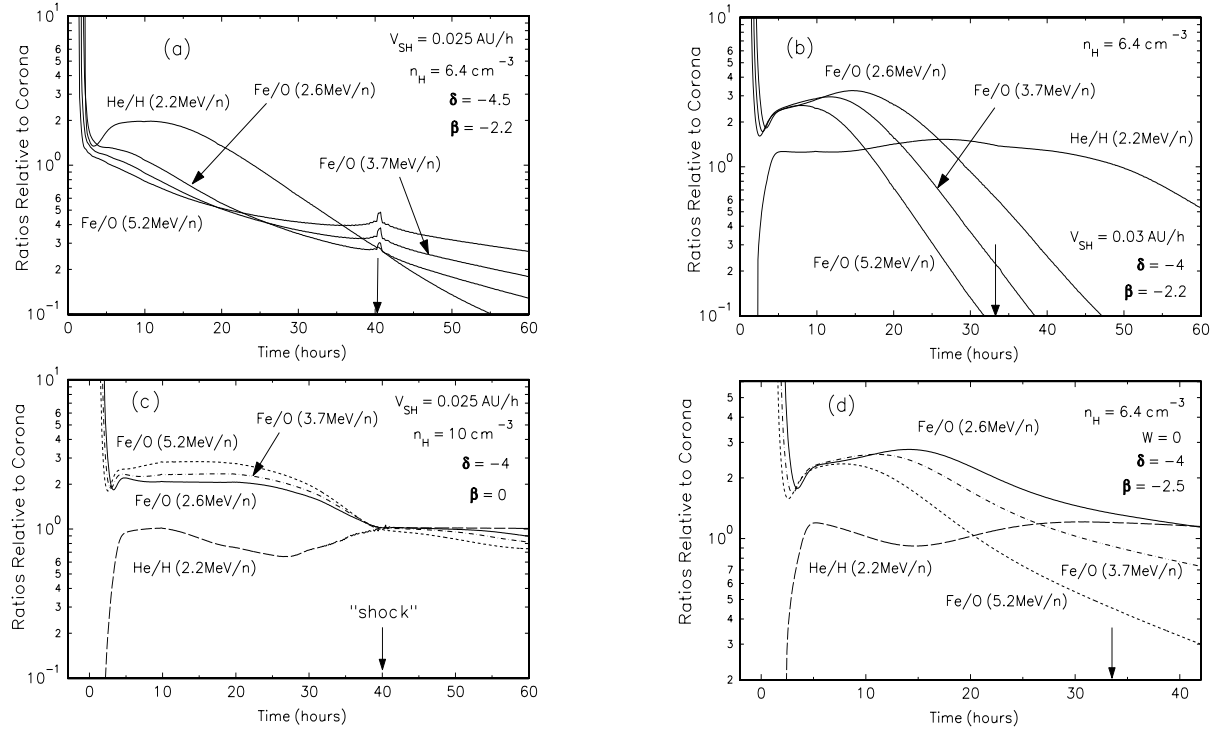


Figure 1: Fe/O and He/H ratios versus time at $r = 1.125$ AU for different source strength of shock-accelerated ions. (a) Initially moderately strong but fast weakening shock. (b) Initially maximum compression but also fast weakening shock. (c) Persistent maximum compression shock. The ion source momentum power-law index is given by $\alpha = \delta + \beta V_{sh} t$ when the shock is at $r_{sh} = r_{0,sh} + tV_{sh}$. (d) Similar to (b), but with no solar-wind convection or wave transport. Vertical arrow indicates shock passage.

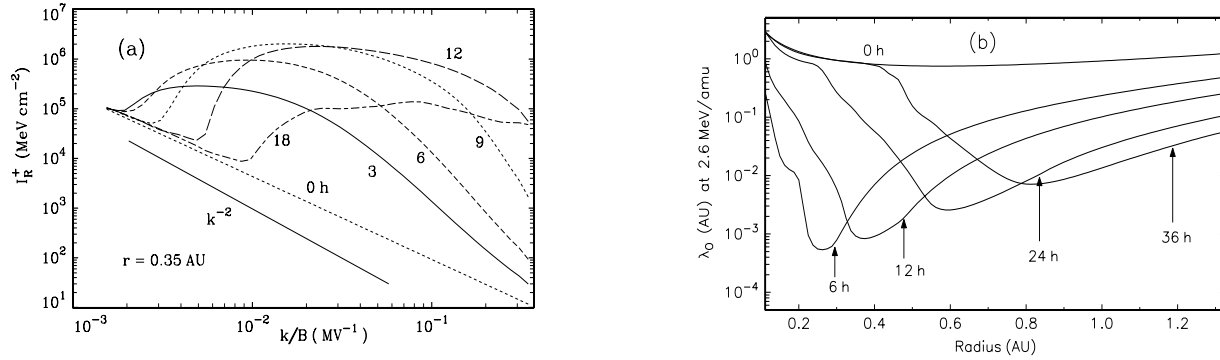


Figure 2: (a) Differential magnetic intensity of forward right-hand Alfvén wave at $r = 0.35$ AU. (b) Evolution of radial profiles of mean free path of 2.6 MeV/amu O^{8+} .

and longer mean free path than H^+ (O^{8+}) in a Kolmogorov wave spectrum, this behavior is at first sight puzzling. In fact, both types of He/H variation at onset (in contrast to the decreasing Fe/O) have been reported (Tylka et al., 1999a,b; Mason et al., 1983, Witte et al., 1979).

For comparison, we display in Fig. 1(d) the results obtained without solar-wind convection and wave transport, with parameters similar to those in Fig. 1(b). The two sets of results are qualitatively similar. However, He/H shows in Fig. 1(d) a valley which is absent in Fig. 1(b). Although we do not display them here, the proton intensity time profiles predicted by the model in these calculations are in the range of the observations.

Fig. 2(a) shows the evolution of right-hand polarized Alfvén wave spectrum at $r = 0.35$ AU from an initial Kolmogorov spectrum, while Fig. 2(b) shows the evolution of the radial profiles of 2.6 MeV/amu oxygen mean free path to $t = 36$ h, both for the parameters of Fig. 1(b). These two figures reveal the dynamic response of Alfvén waves to energetic proton streaming, and argue persuasively that this must have important consequences on SEP transport and abundance evolution.

4 Discussion

The key to understanding the three-stage abundance variations (Fig. 1) with the contrasting behavior between 2.6 MeV/amu Fe/O and 2.2 MeV/amu He/H can be gleaned from Fig. 2, viz. proton excitation of Alfvén waves. The precipitous fall of Fe/O (and He/H if it does) is simply due to propagation effect in the background Kolmogorov wave field ($\propto k^{-5/3}$). For $I_\sigma \propto k^{-b}$, the quasi-linear theory predicts $D_{\mu\mu}/v \propto P^{b-2}$. Hence $D_{\mu\mu}/v$ increases (decreases) with P if $-b$ is $>$ ($<$) -2 at the resonant wavenumber k_{res} . A k^{-2} spectrum is shown in Fig. 2(a) for comparison. The background $k^{-5/3}$ spectrum implies $D_{\mu\mu}/v \propto P^{-1/3}$ everywhere and so Fe/O and He/H will fall precipitously after event onset. However, Fig. 2(a) shows that wave evolution brings in $D_{\mu\mu}/v$ that decreases with P at some k_{res} and increases with P at other k_{res} , in a temporally (and spatially) dependent manner. The rise of He/H may thus be explained as follows. Protons with twice the speed and the same rigidity as 2.2 MeV/amu He²⁺ and $\mu \sim 1$ race ahead at event onset to amplify *en route* Alfvén waves that subsequently scatter the later arriving He²⁺. With sufficiently high proton intensity from a strong shock, this wave growth causes the first “wave” of 2.2 MeV/amu He²⁺ to arrive later than the first “wave” of 2.2 MeV protons, and so He/H rises from < 1 . However, the proton driven wave growth is not large enough at higher rigidities (lower wavenumbers) to reverse the behavior of Fe/O soon after event onset. The rise of Fe/O in the second phase is due to the continuing wave growth retarding O⁸⁺ more than Fe¹⁴⁺. The final decline as the shock approaches is due to more O⁸⁺ being retained near/behind the shock than Fe¹⁴⁺. The later He/H variation may be understood similarly.

We will continue to study the model here to understand its full implications and to delineate its range of validity. We will also extend the model to include nonlinear wave cascading.

AJT acknowledges support from NASA DPR-S92662F.

References

- Barnes, A. 1979, in Solar System Plasma Physics, eds. E. N. Parker et al. Vol. 2 (New York: North Holland), 249
- Lee, M. A. 1983, JGR 88, 6109
- Lee, M. A. 1997, Geophys. Monograph 99, eds. N. Crooker et al. (Washington, DC: AGU), 227
- Mason, G. M., Gloeckler, G., & Hovestadt, D. 1983, ApJ, 267, 844
- Ng, C. K. & Reames, D. V. 1994, ApJ 424, 1032
- Ng, C. K. & Reames, D. V. 1995, ApJ 453, 890
- Ng, C. K., Reames, D. V., & Tylka, A. J. 1999, GRL in press
- Reames, D. V. 1995, Adv. Space Res., 15, 41
- Reames, D. V. 1999, Space Sci. Rev., in press
- Ruffolo, D. 1995, ApJ 442, 861
- Tylka, A. J., Reames, D. V., & Ng, C. K. 1999a, GRL, in press
- 1999b, Proc. 26th ICRC (Salt Lake City, 1999) Paper SH 1.4.19.
- Witte, M., Wibberenz, G., Kunow, H., & Müller-Mellin, R. 1979, Proc. 16th ICRC (Kyoto, 1979), 5, 79